Nonreciprocal Unconventional Photon Blockade with Kerr Magnons

Xiao-Hong Fan,[1] Yi-Ning Zhang,[1] Jun-Po Yu,[2] Ming-Yue Liu,[1] Wen-Di He,[1] Hai-Chao Li,[3,*] and Wei Xiong[1,†]

[1] *Department of Physics, Wenzhou University, Zhejiang 325035, China*
[2] *College of Resources and Environment, Yangtze University, Hubei 430100, China*
[3] *College of Physics and Electronic Science, Hubei Normal University, Huangshi 435002, China*

(Dated: April 26, 2024)

Nonreciprocal devices, allowing to manipulate one-way signals, are crucial to quantum information processing and quantum network. Here we propose a nonlinear cavity-magnon system, consisting of a microwave cavity coupled to one or two yttrium-iron-garnet (YIG) spheres supporting magnons with Kerr nonlinearity, to investigate nonreciprocal unconventional photon blockade. The nonreciprocity originates from the direction-dependent Kerr effect, distinctly different from previous proposals with spinning cavities and dissipative couplings. For a single sphere case, nonreciprocal unconventional photon blockade can be realized by manipulating the nonreciprocal destructive interference between two active paths, via vary the Kerr coefficient from positive to negative, or vice versa. By optimizing the system parameters, the perfect and well tuned nonreciprocal unconventional photon blockade can be predicted. For the case of two spheres with opposite Kerr effects, only reciprocal unconventional photon blockade can be observed when two cavity-magnon coupling strengths Kerr strengths are symmetric. However, when coupling strengths or Kerr strengths become asymmetric, nonreciprocal unconventional photon blockade appears. This implies that two-sphere nonlinear cavity-magnon systems can be used to switch the transition between reciprocal and nonreciprocal unconventional photon blockades. Our study offers a potential platform for investigating nonreciprocal photon blockade effect in nonlinear cavity magnonics.

I. INTRODUCTION

Recently, magnons, also known as spin waves, i.e., the collective spin excitations in ferro- and ferrimagnetic materials like yttrium-iron-garnet (YIG), have attracted considerable attention in condensed matter physics and quantum information science [1–10]. Thanks to the high spin density and low damping of the YIG spheres, photons in microwave cavities can strongly couple to the magnons, giving rise to the field of cavity magnonics [11–13]. Experimentally, sub-millimeter-scale YIG spheres and three-dimensional microwave cavities are frequently employed in cavity magnonics [2–5] for investigating numerous exotic phenomena [11, 14], such as magnon memory [15], spin current [7, 16, 17], entanglement [18–21], dissipative coupling [22–24], blockade [25–27], non-Hermitian physics [28–32], dynamics of polaritons [33], spin interface [34, 35], state manipulation [36–40], microwave-optical transduction [41, 42]. In addition, magnons can strongly interact with superconducting qubits, solid spins, and phonons, building diverse magnon-based hybrid quantum systems including qubit-magnon systems [43–53], cavity magnomechanics [54–57], optomechanical cavity magnonics [58, 60, 61], and cavity optomagnonics [63–65].

With advanced experimental techniques, the magnon Kerr effect (the Kerr nonlinearity of magnons) steming from the magnetocrystalline anisotropy in the YIG [66] has been demonstrated [5, 67], leading to the birth of nonlinear cavity magnonics [68]. Utilizing the magnon Kerr effect, multi-stability [5, 69], magnon entanglement [20], strong spin-spin coupling [50, 51, 70], superradiant phase transition [71], and sensitive detection [72, 73] can be studied. Besides, the magnon Kerr effect can also be used to investigate nonreciprocical devices such as nonreciprocal entanglement [58, 59], nonreciprocal transimission [74], nonreciprocal excitation [75] and nonreciprocal higher-order sideband generation [76]. However, nonreciprocal single-photon blockade has not yet been revealed to date with the magnon Kerr effect, although various nonreciprocal devices have been widely investigated with spinning cavities [77–81] and dissipative coupling [14, 82]. Note that photon blockade is a purely quantum effect, which can be employed to achieve single-photon source devices and generate sub-Poissonian light [83–85]. At present, two classes of photon blockade are proposed: conventional [86–88] and unconventional [89–94] photon blockade. The former is caused by strong anharmonicity of the eigenenergy spectrum, and the latter is formed by the destructive quantum interference in different transition paths under weak nonlinearity.

Here, we propose a scheme to realize a nonreciprocal unconventional single-photon blockade in a Kerr-modified cavity-magnon system, which consists of a microwave cavity coupled to one or two YIG spheres supporting Kerr magnons. The nonreciprocity is induced by the direction-dependent Kerr nonlinearity. Specifically, when the biased magnetic field is alinged along the crystal axis [100] ([110]), the Kerr coefficient is positive (negative), which has been demonstrated experimentally [67]. In the case of a single sphere in the cavity, only two interference passages are activated. By changing the Kerr coefficient from positive to negative (or vice versa), non-

*hcl2007@foxmail.com
†xiongweiphys@wzu.edu.cn

reciprocal destructive interference occurs, leading to the manifestation of nonreciprocal photon blockade. This phenomenon can be rigorously demonstrated through both analytical and numerical analyses, focusing on the equal-time second-order correlation function. When the system parameters are optimized, achieving the (ideal) perfect nonreciprocal photon blockade becomes feasible. Additionally, we illustrate that the degree of nonreciprocity can be finely tuned by manipulating system parameters, as evidenced by the study of the defined contrast ratio. When two spheres with opposite Kerr coefficients are considered, three active interference passages emerge. In the case of symmetrical coupling strengths and Kerr coefficients, two passages induced by magnon-photon couplings assume identical roles in destructively interfering with the passage created by the pumping field, thereby leading to reciprocal photon blockade. When two cavity-magnon coupling strengths or Kerr coefficients become asymmetric, two passages activated by the coupling strengths assume distinct roles in interfering with the pumping passage, resulting in nonreciprocal photon blockade, as evidenced by the corresponding contrast ratio. This indicates that two-sphere nonlinear cavity-magnon systems can be used to switch the transition between reciprocal and nonreciprocal photon blockades. Our investigation opens up a promising avenue for engineering nonreciprocal devices in both single and multiple YIG spheres with magnon Kerr effect.

The rest paper is organized as follows: In Sec. II, the model is described, and the effective non-Hermitian Hamiltonian is given. Then we study the nonreciprocal photon blockade in a cavity including a single sphere in Sec. III. In Sec. IV, we further study the nonreciprocal photon blockade in a cavity including two symmetric and asymmetric spheres. Finally, a conclusion is given in Sec. V.

II. MODEL AND HAMILTONIAN

We consider a nonlinear cavity magnonics consisting of one or two YIG spheres coupled to a microwave cavity [see Fig. 1(a)], where the Kittel mode of the YIG sphere is used to support the Kerr magnons (i.e., magnons with the Kerr effect). Such the nonlinearity, arising from the magnetocrystallographic anisotropy, can be tuned by the direction of the magnetic field [32, 67]. Specifically, the Kerr coefficient is positive (negative) when the magnetic field is aligned along with the crystallographic axis [100] ([110]) of the YIG sphere. For studying photon blockade effect, an additional pumping field with the frequency ω_p and the Rabi frequency Ω is imposed to the microwave cavity. The Hamiltonian of the proposed system can be written as (setting $\hbar = 1$),

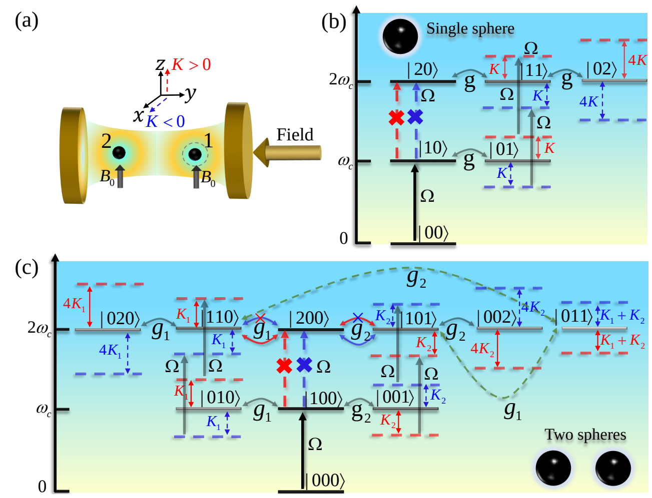

FIG. 1: (a) Schematic diagram of the proposed cavity-magnon system. It consists of one or two YIG spheres supporting Kerr magnons coupled to a pumped cavity. The YIG sphere(s) is (are) placed in a static magnetic field B_0, along the crystallographic axis [100] or [110]. Correspondingly, $K > 0$ or $K < 0$. (b) Energy level diagram of a single sphere coupled to a cavity and the corresponding excitation paths. (c) Energy level diagram of two spheres simultaneously coupled to a common cavity and the corresponding excitation paths.

$$H_{\rm sys} = \sum_{j=1,2}[\omega_m m_j^\dagger m_j + g_j(m_j^\dagger c + c^\dagger m_j) + K_j(m_j^\dagger m_j)^2] + \omega_c c^\dagger c + \Omega(c e^{i\omega_p t} + c^\dagger e^{-i\omega_p t}), \tag{1}$$

where $\omega_{c(m)}$ is the resonance frequency of the photons (magnons) in the cavity (Kittel) mode, g_j is the photon-magnon coupling strength and K is the Kerr coefficient. The operators c (m_j) and $c^\dagger$ ($m_j^\dagger$) are the annihilation and creation operators of the photons (jth magnon). In the rotating frame with respect to ω_p, Eq. (1) reduces to

$$H_{\rm rf} = \sum_{j=1,2}[\Delta_m m_j^\dagger m_j + g_j(m_j^\dagger c + c^\dagger m_j) + K_j(m_j^\dagger m_j)^2] + \Delta_c c^\dagger c + \Omega(c + c^\dagger), \tag{2}$$

where $\Delta_{c(m)} = \omega_{c(m)} - \omega_p$ is the frequency detuning of the photons (magnons) from the pumping field.

By further taking the dissipations of the system into account and neglecting the quantum jump terms, the effective non-Hermitian Hamiltonian of the system is

$$H_{\rm eff} = H_{\rm rf} - i\frac{\kappa_c}{2}c^\dagger c - i\sum_{j=1,2}\frac{\kappa_m}{2}m_j^\dagger m_j, \tag{3}$$

where κ_c and κ_m are the decay rates of the photons and magnons, respectively.

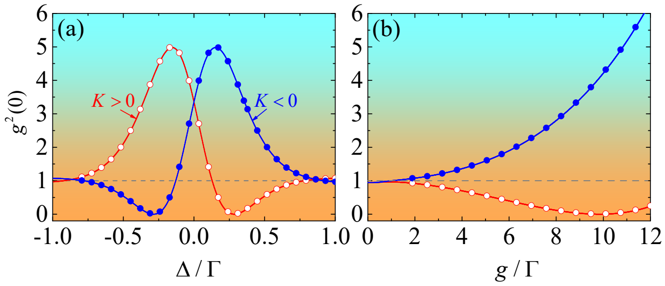

FIG. 2: $g^2(0)$ versus the normalized (a) detuning Δ and (b) magnon-photon coupling strength g. The red (blue) curve corresponds to the case of $K>0$ ($K<0$). In (a), $g=g_{\rm opt}=9.88\Gamma$, and in (b), $\Delta=\Delta_{\rm opt}=0.287\Gamma$. Other parameters are $\Gamma/2\pi=1$ MHz, $|K|/\Gamma=4\times10^{-3}$, and $\Omega/\Gamma=0.1$.

III. NONRECIPROCAL PHOTON BLOCKADE WITH A SINGLE SPHERE

In this section, we investigate the photon blockade in the proposed system consisting of a single YIG sphere coupled to the cavity, i.e., $j=1$ in Eq. (1). The magnon-photon coupling strength and the magnon Kerr coefficient are respectively denoted by $g_1=g$ and $K_1=K$. Our analysis focuses on the equal-time second-order correlation function of the photons in the cavity. The Fock-state basis of the system is denote by $|nm\rangle=|n\rangle\otimes|m\rangle$, with n being the number of photons in the microwave cavity and m the number of magnon. In the weak pumping regime, $\Omega/\kappa_{c(m)}\ll1$, the photon number is small, so we can work within the few-photon subspace spanned by the basis states $|0\rangle_c$, $|1\rangle_c$, and $|2\rangle_c$. Therefore, the state of the system at arbitrary time can be expressed as

$$\begin{aligned}|\psi_t\rangle=&C_{00}|0\rangle_c|0\rangle_m+C_{10}|1\rangle_c|0\rangle_m+C_{01}|0\rangle_c|1\rangle_m\\&+C_{20}|2\rangle_c|0\rangle_m+C_{11}|1\rangle_c|1\rangle_m+C_{02}|0\rangle_c|2\rangle_m,\end{aligned}\quad(4)$$

where C_{ij} with $i,j=0,1,2$ are the probability amplitudes. By substituting the state $|\psi_t\rangle$ into the Schrödinger equation, the following equations of motion for the probability amplitudes can be obtained,

$$\begin{aligned}i\dot{C}_{00}=&\Omega C_{10},\\i\dot{C}_{10}=&\Delta_c'C_{10}+gC_{01}+\sqrt{2}\Omega C_{20}+\Omega C_{00},\\i\dot{C}_{01}=&gC_{10}+(\Delta_m'+K)C_{01}+\Omega C_{11},\\i\dot{C}_{20}=&2\Delta_c'C_{20}+\sqrt{2}\Omega C_{10}+\sqrt{2}gC_{11},\\i\dot{C}_{11}=&\Omega C_{01}+\sqrt{2}g(C_{20}+C_{02})+(\Delta_c'+\Delta_m'+K)C_{11},\\i\dot{C}_{02}=&\sqrt{2}gC_{11}+2(\Delta_m'+2K)C_{02},\end{aligned}\quad(5)$$

where $\Delta'_{c(m)}=\Delta_{c(m)}-i\kappa_{c(m)}/2$. In the long-time limit, the probalitity amplitudes can be attained by directly solving $\dot{C}_{ij}=0$.

When the system is in the state (4), the equal-time second-order correlation function of the photons can be calculated as

$$g^2(0)\equiv\frac{\langle c^\dagger c^\dagger cc\rangle}{\langle c^\dagger c\rangle^2}=\frac{2|C_{20}|^2}{(|C_{10}|^2+|C_{11}|^2+2|C_{20}|^2)^2}.\quad(6)$$

In the weak pumping regime ($\Omega\ll\Gamma$), we have $|C_{10}|^2\gg|C_{11}|^2,|C_{20}|^2$. This means that the probability of finding one photon in the cavity is much larger than that of simultanesouly finding one photon and one magnon, which is also much larger than that of finding two photons in the cavity. As a result, $g^2(0)\approx2|C_{20}|^2/|C_{10}|^4<1$, i.e., the photon blockade is achieved. Since the probabilities in Eq. (6) are affected by the magnon Kerr effect (K) [see Eq. (5)], the so-called nonreciprocal photon blockade can be achieved via changing the direction of the magnetic field (i.e., $K>0$ or $K<0$). To show this, we analytically plot the equal-time second-order correlation $g^2(0)$ versus the normalized detuning Δ/Γ and coupling strength g/Γ in Fig. 2, where $\omega_c=\omega_m=\omega$ (equivalently, $\Delta_c=\Delta_m=\Delta$) and $\kappa_c=\kappa_m=\Gamma$ are assumed for simplicity hereafter. The red (blue) curve denotes $K>0$ ($K<0$), corresponding to the case that the magnetic field is aligned along the crystal axis [100] ([110]). From Fig. 2(a), we show that the perfect photon blockade can be realized by tuning Δ when the magnon-photon coupling strength g is fixed at its optimal value. For $K>0$ and $K<0$, the nonreciprocal photon blockade is predicted. When the positive optimal value of the detuning $\Delta_{\rm opt}/\Gamma=0.287$ is chosen [see Fig. 2(b)], $g^2(0)$ decreases first from $g^2(0)=1$ to $g^2(0)=0$ and then increases with increasing g when $K>0$. But when $K<0$, $g^2(0)$ monotonically increases, resulting in photon bunching [$g^2(0)>1$]. To demonstrate the validity of our approximate analysis, we also perform the numerical simulation by using the Lindblad master equation

$$\dot{\rho}=i[\rho,H_{\rm rf}]+\frac{\kappa_c}{2}\mathcal{L}[c]\rho+\frac{\kappa_m}{2}\mathcal{L}[m]\rho,\quad(7)$$

where ρ is the density matrix of the considered system, $\mathcal{L}[o]\rho=2o\rho o^\dagger-o^\dagger o\rho-\rho o^\dagger o$ is the Lindblad operator. Obviously, the analytical result well matches the simulation (see the circles and squares in Fig. 2). The mechanism of the photon blockade can be explained by the destructive interference between two transition paths [see Fig. 1(b)]. One path is formed by directly pumping the vaccum cavity to the cavity having two photons, i.e., $|0\rangle_c|0\rangle_m\to|1\rangle_c|0\rangle_m\to|2\rangle_c|0\rangle_m$. The other path is formed by the strong coupling between the magnons and photons. Specifically, when one photon is excited in the cavity, the magnon-photon coupling leads to the transition between the states $|1\rangle_c|0\rangle_m$ and $|0\rangle_c|1\rangle_m$. Then the pumpling field excites the state $|0\rangle_c|1\rangle_m$ to the state $|1\rangle_c|1\rangle_m$. Due to the photon-magnon coupling, the state $|1\rangle_c|1\rangle_m$ further transits to the states $|2\rangle_c|0\rangle_m$ and $|0\rangle_c|2\rangle_m$. During these transitions, the frequency shift induced by the magnon Kerr effect is positive (negative) for $K>0$ ($K<0$). This indicates when the photon blockade is achieved at $K>0$ ($K<0$) for fixed parameters, the reversed photon bunching, i.e.,

$g^2(0) > 1$, is predicted at $K < 0$ ($K > 0$), as demonstrated in Fig. 2(a).

From Fig. 2, one can find that the optimal coupling strength $g_{\rm opt}$ and frequency detuning $\Delta_{\rm opt}$ for a given K must exist for prediction of the perfect photon blockade [$g^2(0) = 0$]. This indicates that the probability of simultaneously finding two photons in the cavity is nearly zero [see Eq. (6)], i.e., $|C_{20}|^2 \approx 0$, which can be directly convinced by the simulation results in Fig. 3. To analytically obtain the optimal parameters, the perfect photon blockade condition can be specifically rewritten as

$$\frac{g^2 K}{\Delta_m' + 2K} + (\Delta_c' + \Delta_m' + K)(\Delta_m' + K) = \Omega^2, \tag{8}$$

or equivalently,

$$\begin{aligned} 2\Omega^2 + \Gamma^2 =& 12\Delta^2 + 28\Delta K + 14K^2, \\ \frac{g^2 K}{4\Delta + 3K} =& (\Delta + 2K)^2 + \Gamma^2/4. \end{aligned} \tag{9}$$

From the second equality in Eq. (9), the inequality

$$(4\Delta + 3K)K > 0 \tag{10}$$

can be directly obtained for a given g. This means that the perfect photon blockade can only be predicted in the region of $\Delta > -3K/4$ ($< -3K/4$) for $K > 0$ (< 0). In addition, the optimal coupling strength

$$g_{\rm opt} = \sqrt{\frac{4\Delta_{\rm opt} + 3K}{K}[(\Delta_{\rm opt} + 2K)^2 + \Gamma^2/4]} \tag{11}$$

is required to realize perfect photon blockade for a given K, where the optimal paramter $\Delta_{\rm opt}$ is given by the first equality in Eq. (9), i.e.,

$$\Delta_{\rm opt} = \frac{-7K \pm \sqrt{7K^2 + 6\Omega^2 + 3\Gamma^2}}{6} \approx \pm\frac{\sqrt{3}}{6}\Gamma. \tag{12}$$

The second approximate equality is established because $K, \Omega \ll \Gamma$ is taken. The sign '+ ($-$)' corresponds to $K > 0$ (< 0).

To quantitatively charaterize the nonreciprocal photon blockade, a bidirectional contrast ratio is introduced, i.e.,

$$C = \left|\frac{g^2_{K>0}(0) - g^2_{K<0}(0)}{g^2_{K>0}(0) + g^2_{K<0}(0)}\right| \in [0, 1], \tag{13}$$

where $C = 1$ (0) denotes the ideal nonreciprocal (reciprocal) photon blockade. The larger the contrast ratio C, the stronger the nonreciprocity of the photon blockade. In Fig. 4(a), we show the behavior of the contrast ratio with the normalized detuning Δ/Γ with different magnon-photon couplings. Clearly, the nonreciprocity and reciprocity for the photon blockade can be switched by tuning the detuning Δ. When the coupling strenth is optimal (i.e., $g_{\rm opt} = 9.88\Gamma$), the ideal nonreciprocal photon blockade can be attained. But when the coupling strength deviates from the optimal value such as

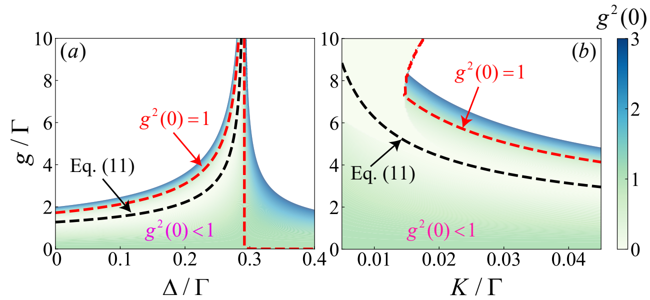

FIG. 3: (a) Density plot of $g^2(0)$ vs the normalized coupling strength g/Γ and the normalized detuning Δ/Γ. (b) Density plot of $g^2(0)$ vs the normalized coupling strength g/Γ and the normalized Kerr coefficient K/Γ. In panels (a) and (b), the red dashed curve denotes $g^2(0) = 1$, the black dashed curve satisfies the optimal conditon in Eq. (11), and the light green zone means photon blockade, i.e., $g^2(0) < 1$. Other parameters are the same as those in Fig. 2.

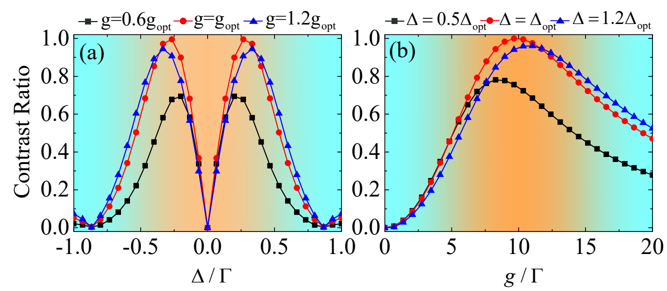

FIG. 4: (a) The contrast ratio C versus the normalized detuning Δ with different magnon-photon coupling strengths $g = g_{\rm opt} = 9.88\Gamma$ (red), $0.6g_{\rm opt}$ (black), and $1.2g_{\rm opt}$ (blue). (b) The contrast ratio C versus the normalized coupling strength g with different detunings $\Delta = \Delta_{\rm opt} = 0.287\Gamma$ (red), $0.5\Delta_{\rm opt}$ (black), and $1.2\Delta_{\rm opt}$ (blue). Other parameters are the same as those in Fig. 2.

$g = 0.6g_{\rm opt}$ and $g = 1.2g_{\rm opt}$, the maximum nonreciprocity of the photon blockade has a different degree of reduction (see curves marked by squares and triangles). In Fig. 4(b), we also investigate the contrast ratio with the normalized coupling strength g/Γ with different detunings. By increasing g, one can see that the contrast ratio increases first to its maximum and then decreases. At the optimal detuning $\Delta_{\rm opt} = 0.287\Gamma$, the ideal nonreciprocal photon blockade ($C = 1$) is predicted. Deviating from this optimal value such as $\Delta = 0.5\Delta_{\rm opt}$ (the black curve with squares) and $\Delta = 1.2\Delta_{\rm opt}$ (the blue curve with triangles), the maximum nonreciprocity of the photon blockade reduces.

IV. NONRECIPROCAL PHOTON BLOCKADE WITH TWO SPHERES

We next study the photon blockade in the considered system consisting of two YIG spheres simultanesouly cou-

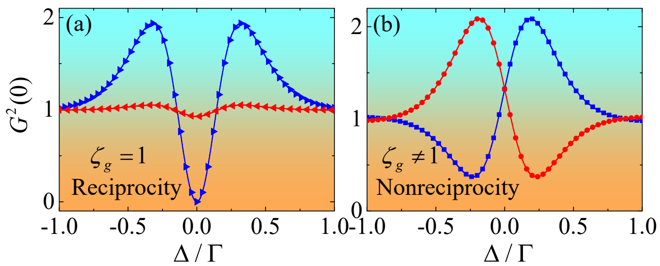

FIG. 5: $G^2(0)$ versus the normalized detuning Δ with (a) $g_1 = g_2$ and (b) $g_1 \neq g_2$ in the case of $\zeta_K < 0$. In (a), the red (blue) curve corresponds to $g_1 = g_2 = 15\Gamma$ ($= g_{\rm opt} = 63\Gamma$). Other parameters are the same as those in Fig. 2.

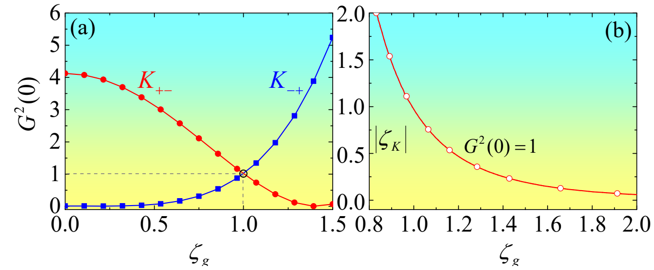

FIG. 6: (a) $G^2(0)$ versus the relative coupling strength ζ_g with $\Delta = -0.287\Gamma$ in the case of $\zeta_K < 0$, where the red (blue) curve corresponds to K_{+-} (K_{-+}). (b) The contourplot of $G^2(0) = 1$ versus ζ_g and $|\zeta_K|$. Other parameters are the same as those in Fig. 2.

pled to a cavity [see Eq. (3) with $j = 2$]. For conveniance, we define two parameters $\zeta_g = g_1/g_2$ and $\zeta_K = K_1/K_2$ as the relative coupling strength and Kerr coefficient, respectively. In the weak pumping regime, the state of the considered system governed by Eq. (3) with $j = 2$ becomes

$$\begin{aligned}|\psi_t'\rangle =&C_{000}|000\rangle + C_{001}|001\rangle + C_{100}|100\rangle + C_{010}|010\rangle\\ &+C_{200}|200\rangle + C_{110}|110\rangle + C_{011}|011\rangle + C_{101}|101\rangle\\ &+C_{020}|020\rangle + C_{002}|002\rangle \end{aligned}\tag{14}$$

when the system is initially prepared in the state $|0\rangle_c|0\rangle_1|0\rangle_2$, where the subscripts c, 1 and 2 denote the cavity mode, the spheres 1 and 2. Following the procedure of calculating the equal-time second-order correlation fuction in the case of a single sphere, we have

$$G^2(0) = \frac{2|C_{200}|^2}{(|C_{100}|^2 + |C_{110}|^2 + |C_{101}|^2 + 2|C_{200}|^2)^2},\tag{15}$$

which charaterizes the equal-time second-order correlation fuction in the presence of two YIG spheres. Here we have used the approximation $|C_{200}|^2 \ll |C_{110}|^2, |C_{101}|^2 \ll |C_{100}|^2$. This directly leads to photon blockade, i.e., $G^2(0) < 1$. To address this, we further consider the following two scenarios: (i) The directions of two magnetic fields are identical ($\zeta_K > 0$); (ii) the directions of two magnetic fields are opposite ($\zeta_K < 0$). When $\zeta_K > 0$, the predicted nonreciprocal photon blockade is similar to that of a single sphere (see Fig. 2), which has been numerically checked. Therefore, we do not provide discussions here anymore.

Interestingly, the situation of $\zeta_K < 0$ is completely different from that of $\zeta_K > 0$. For simplicity, we assume that the magnons in two spheres have the same absolute values, i.e., $|\zeta_K| = 1$, equivalently $|K_1| = |K_2|$. In the following discussion, we label the scenario of $K_1 > 0$ and $K_2 < 0$ ($K_1 < 0$ and $K_2 > 0$) as K_{+-} (K_{-+}). When the magnons in two YIG spheres are identically coupled to the cavity ($\zeta_g = 1$), only the reciprocal photon blockade is predicted for K_{+-} and K_{-+} [see red or blue curve in Fig. 5(a)]. This is due to the fact that the transitions $|000\rangle \to |100\rangle \to |001\rangle \to |101\rangle \to |200\rangle$ and $|000\rangle \to |100\rangle \to |010\rangle \to |110\rangle \to |200\rangle$ play the same role in destructively interfering with the transition $|000\rangle \to |100\rangle \to |200\rangle$ when $\zeta_g = 1$ and $|\zeta_K| = 1$ [see Fig. 1(c)]. To obtain a *visible* photon blockade [$G^2(0) \ll 1$], the large magnon-coupling strengths are needed. At the optimal coupling strength $g_{\rm opt} = 63\Gamma$, we find that the perfect photon blockade is achieved at $\Delta_{\rm opt} = 0$, as shown by the blue curve in Fig. 5(a). This optimal coupling strength can be experimentally realized owing to the achieved strong and ultra-strong photon-magnon interactions [3, 95, 96]. However, when $\zeta_g \neq 1$ (i.e., $g_1 \neq g_2$), the nonreciprocal photon blockade is clearly observed [see Fig. 5(b)], where the red (blue) curve corresponds to K_{+-} (K_{-+}). To realize this nonreciprocal photon blockade, the required magnon coupling strength is relatively smaller than that of $\zeta_g = 1$. This means that the nonreciprocal photom blockade can be engineered by using the asymmetric and relatively small magnon-photon coupling strength, making the proposal more feasible in experiments. At $\Delta/\Gamma = +2.87$ (-2.87), the optimal photon blockade occurs for K_{+-} (K_{-+}). The mechanism of the nonreciprocal photon blockade at $\zeta_g \neq 1$ can be interpreted as follows: For K_{+-} [see the red levels in Fig. 1(c)], the transition $|000\rangle \to |100\rangle \to |010\rangle \to |110\rangle \to |200\rangle$ is allowed at $\Delta > 0$, while the transtion $|000\rangle \to |100\rangle \to |001\rangle \to |101\rangle \to |200\rangle$ is forbidden due to the Kerr effect induced large detuning. As a result, the photon blockade is caused by the destructive interference between the former and the direct pumping path $|000\rangle \to |100\rangle \to |200\rangle$. On the contrary, the transition $|000\rangle \to |100\rangle \to |010\rangle \to |110\rangle \to |200\rangle$ is forbidden at $\Delta < 0$, while the transtion $|000\rangle \to |100\rangle \to |001\rangle \to |101\rangle \to |200\rangle$ is allowed, giving rise to photon blockade for K_{-+} [see the blue levels in Fig. 1(c)].

Figure 6(a) further examines the behavior of the photon blockade with the relative coupling strength ζ_g, where $g_2/\Gamma = 9.88$ is fixed. In the absence of one sphere such as the sphere 1 ($\zeta_g = 0$), the photons in the cavity is bunching (antibunching) for the case of K_{+-} (K_-+). By coupling the sphere 1 to the cavity and continuously increasing g_1, we find that the property of the statistic photons are changed from bunching to antibunching

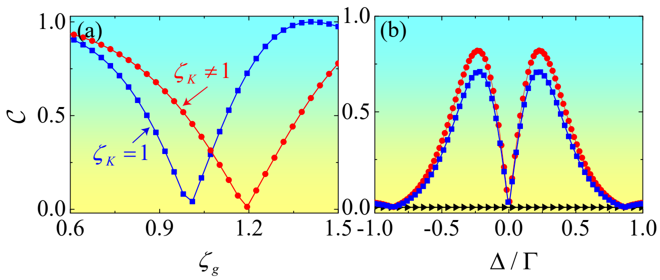

FIG. 7: The contrast ratio $\mathcal{C}$ versus (a) the relative coupling strength ζ_g and (b) the normalized detuning Δ. In (a), $\zeta_K = 1$ with $|K_1| = |K_2| = 4 \times 10^{-3}\Gamma$ (blue) and $\zeta_g \neq 1$ with $|K_2| = 2|K_1| = 4\times10^{-3}\Gamma$ (red). In (b), the black curve denotes $g_1 = g_2 = 9.88\Gamma$ and $|K_1| = |K_2| = 4\times10^{-3}$, the red curve denotes $g_1/\Gamma = 12$, $g_2/\Gamma = 9.88$, and $|K_1| = |K_2| = 4\times10^{-3}$, the blue curve denotes $g_1 = g_2 = 9.88\Gamma$ and $|K_2| = 4|K_1| = 4 \times 10^{-3}$. Other parameters are the same as those in Fig. 2.

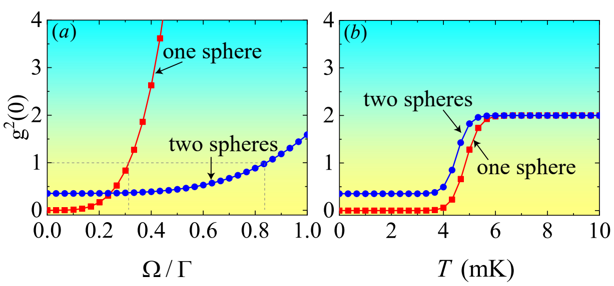

FIG. 8: The second-order correlation function $g^2(0)$ vs (a) the normalized Rabi frequency of the pumping field and (b) the bath temperature, where the red (blue) curve denotes the case of the single sphere (two spheres). Other parameters are the same as those in Fig. 2.

(blockade) for K_{+-}, and conversely, from antibunching to bunching for K_{-+}. This indicates that the nonreciprocal photon blockade can be achieved in a broad range of the parameter ζ_g. Note that at $\zeta_g = 1$ ($g_1 = g_2 = 9.88\Gamma$), $G^2(0) = 1$ for both K_{+-} and K_{-+} (see the crosspoint), meaning that the nonreciprocity disappears and photons satisfies Poissionian distribution. Figure 6(b) reveals the relationship between ζ_g and $|\zeta_K|$ when $G^2(0) = 1$. With increasing ζ_g, the relative Kerr coefficient decreases. This suggests that the crosspoint in Fig. 6(a) has a right (left) shift with increasing (decreasing) ζ_g when $|\zeta_K| < 1$ (> 1).

To describe the nonreciprocity of the photon blockade induced by the opposite Kerr effects of the magnons in two spheres, a contrast ratio $\mathcal{C}$ is defined as

$$\mathcal{C} = \left| \frac{G^2_{K_{+-}}(0) - G^2_{K_{-+}}(0)}{G^2_{K_{+-}}(0) + G^2_{K_{-+}}(0)} \right|. \tag{16}$$

In Fig. 7, we respectively plot it versus the relative coupling strength ζ_g and the normalized detuning Δ/Γ. One can see that the nonreciprocity can be well tuned between 0 (reciprocity) and 1 (nonreciprocity) by the relative coupling strength ζ_g in Fig. 7(a) when $|\zeta_K| = 1$. In particular, the nonreciprocity disappears at $\zeta_g = 1$, consistent with above discussions. To recover the nonreciprocity, aysmmetric coupling strengths ($\zeta_g \neq 1$) or Kerr coefficents ($|\zeta_K| \neq 1$) can be employed, as demonstrated by the the blue and red curves, respectively. Obviously, the nonreciprocity of the photon blockade can also be controlled by ζ_g for the asymmetric Kerr coefficents ($|\zeta_K| \neq 1$). When the magnon-photon coupling strenghts are fixed, the contrast ratio can be tuned by the normalized detuning Δ/Γ in Fig. 7(b). Specifically, only reciprocal photon blockade is predicted ($\mathcal{C} = 0$) at $\zeta_g = 1$, $|\zeta_K| = 1$ (see the black curve). However, one of the conditions is broken, i.e., $\zeta_g \neq 1$ and $|\zeta_K| = 1$, or $\zeta_g = 1$ and $|\zeta_K| \neq 1$, the nonreciprocity of the photon blockade can be observed.

V. DISCUSSION AND CONCLUSION

Before concluding, we give a brief study of the Rabi frequency of the weak pumping field and the effect of the bath temperature on the photon blockade. From Fig. 8(a), one can see that the photon blockade can be realized at $\Omega < 0.31\Gamma$ ($\Omega < 0.84\Gamma$) in the presence of single YIG sphere (two YIG spheres). This indicates that the range of Ω for achieving the photon blockade can be widened via increasing the number of YIG spheres. Figure 8(b) shows the impact of the bath temperature on the photon blockade. Obviously, $g^2(0)$ is nearly unchanged when $T < 4$ mK for both the cases of single sphere and two spheres. But when the temperature crosses the point $T = 4$ mK, $g^2(0)$ has a sudden increase. For the case of single sphere (two spheres), photon blockade disappears when $T > 4.45$ mK ($T > 4.5$ mK). It is also evident that the proposed system including one sphere can have better photon blockade effect than the case of two spheres at a certain temperature.

In summary, we have proposed a nonlinear cavity-magnon system to study the nonreciprocal photon blockade. The nonreciprocity stems from the direction-dependent Kerr effect of magnons in the YIG sphere. For a single sphere case, the nonreciprocal destructive interference between two paths leads to nonreciprocal photon blockade by varying the Kerr coefficient from positive to negative (or vice versa). By optimizing the system parameters, perfect nonreciprocal photon blockade can be predicted and finely tuned. For the case of two spheres with opposite Kerr coefficients, only reciprocal photon blockade can be predicted when two cavity-magnon coupling strengths and Kerr coefficients are symmetric. However, when two coupling strengths or Kerr coefficients becomes asymmetric, nonreciprocal photon blockade appears. This indicates that the transition between reciprocity and nonreciprocity of photon blockade can be arbitrarily switched in a two-sphere cavity-magnon system. Our study paves a potential way to engineer nonreciprocal devices in nonlinear cavity magnonics.

This work was supported by Zhejiang Provincial Natural Science Foundation of China under Grant No. LY24A040004, the National Natural Science Foundation of China under Grant No. 11804074, and the Natural Science Foundation of Hubei Province of China under Grant No. 2022CFB509.

[1] H. Huebl, C. W. Zollitsch, J. Lotze, F. Hocke, M. Greifenstein, A. Marx, R. Gross, and S. T. B. Goennenwein, High Cooperativity in Coupled Microwave Resonator Ferrimagnetic Insulator Hybrids, Phys. Rev. Lett. **111**, 127003 (2013).

[2] Y. Tabuchi, S. Ishino, T. Ishikawa, R. Yamazaki, K. Usami, and Y. Nakamura, Hybridizing Ferromagnetic Magnons and Microwave Photons in the Quantum Limit, Phys. Rev. Lett. **113**, 083603 (2014).

[3] X. Zhang, C.-L. Zou, L. Jiang, and H. X. Tang, Strongly Coupled Magnons and Cavity Microwave Photons, Phys. Rev. Lett. **113**, 156401 (2014).

[4] M. Goryachev, W. G. Farr, D. L. Creedon, Y. Fan, M. Kostylev, and M. E. Tobar, High-Cooperativity Cavity QED with Magnons at Microwave Frequencies, Phys. Rev. Applied **2**, 054002 (2014).

[5] Y. P. Wang, G. Q. Zhang, D. Zhang, X. Q. Luo, W. Xiong, S. P. Wang, T. F. Li, C. M. Hu, and J. Q. You, Magnon Kerr effect in a strongly coupled cavity-magnon system, Phys. Rev. B **94**, 224410 (2016).

[6] B. Bhoi, T. Cliff, I. S. Maksymov, M. Kostylev, R. Aiyar, N. Venkataramani, S. Prasad, and R. L. Stamps, Study of photon–magnon coupling in a YIG-film split-ring resonant system, J. Appl. Phys. **116**, 243906 (2014).

[7] L. Bai, M. Harder, Y. P. Chen, X. Fan, J. Q. Xiao, and C.-M. Hu, Spin Pumping in Electrodynamically Coupled Magnon-Photon Systems, Phys. Rev. Lett. **114**, 227201 (2015).

[8] D. Zhang, X. M. Wang, T. F. Li, X. Q. Luo, W. Wu, F. Nori, and J. Q. You, Cavity quantum electrodynamics with ferromagnetic magnons in a small yttrium-iron-garnet sphere, npj Quantum Inf. **1**, 15014 (2015).

[9] Y. Li, T. Polakovic, Y.-L. Wang, J. Xu, S. Lendinez, Z. Zhang, J. Ding, T. Khaire, H. Saglam, R. Divan, J. Pearson, W.-K. Kwok, Z. Xiao, V. Novosad, A. Hoffmann, and W. Zhang, Strong Coupling between Magnons and Microwave Photons in On-Chip Ferromagnet-Superconductor Thin-Film Devices, Phys. Rev. Lett. **123**, 107701 (2019).

[10] J. T. Hou and L. Liu, Strong Coupling between Microwave Photons and Nanomagnet Magnons, Phys. Rev. Lett. **123**, 107702 (2019).

[11] B. Z. Rameshti, S. V. Kusminskiy, J. A. Haigh, K. Usami, D. Lachance-Quirion, Y. Nakamura, C. M. Hu, H. X. Tang, G. E. W. Bauer, and Y. M. Blanter, Cavity magnonics, Phys. Rep. **979**, 1 (2022).

[12] D. Lachance-Quirion, Y. Tabuchi, A. Gloppe, K. Usami, and Y. Nakamura, Hybrid quantum systems based on magnonics, Appl. Phys. Express **12**, 070101 (2019).

[13] H. Y. Yuan, Y. Cao, A. Kamra, R. A. Duine, and P. Yan, Quantum magnonics: When magnon spintronics meets quantum information science, Phys. Rep. **965**, 1 (2022).

[14] Y. P. Wang and C.-M. Hu, Dissipative couplings in cavity magnonics, J. Appl. Phys. **127**, 130901 (2020).

[15] X. Zhang, C.-L. Zou, N. Zhu, F. Marquardt, L. Jiang, and H. X. Tang, Magnon dark modes and gradient memory, Nat. Commun. **6**, 8914 (2015).

[16] L. Bai, M. Harder, P. Hyde, Z. Zhang, C. M. Hu, Y. P. Chen, and J. Q. Xiao, Cavity Mediated Manipulation of Distant Spin Currents Using a Cavity-Magnon-Polariton, Phys. Rev. Lett. **118**, 217201 (2017).

[17] D. Mukhopadhyay, J. M. P. Nair, and G. S. Agarwal, Quantum amplification of spin currents in cavity magnonics by a parametric drive induced long-lived mode, Phys. Rev. B **106**, 184426 (2022).

[18] H. Y. Yuan, S. Zheng, Z. Ficek, Q. Y. He, and M.-H. Yung, Enhancement of magnon-magnon entanglement inside a cavity, Phys. Rev. B **101**, 014419 (2020).

[19] V. A. Mousolou, Y. Liu, A. Bergman, A. Delin, O. Eriksson, M. Pereiro, D. Thonig, and E. Sjöqvist, Phys. Magnon-magnon entanglement and its quantification via a microwave cavity, Phys. Rev. B **104**, 224302 (2021).

[20] Z. Zhang, Marlan O. Scully, and Girish S. Agarwal, Quantum entanglement between two magnon modes via Kerr nonlinearity driven far from equilibrium, Phys. Rev. Research **1**, 023021 (2019).

[21] Y. Ren, J. Xie, X. Li, S. Ma, and F. Li, Long-range generation of a magnon-magnon entangled state, Phys. Rev. B **105**, 094422 (2022).

[22] M. Harder, Y. Yang, B. M. Yao, C. H. Yu, J. W. Rao, Y. S. Gui, R. L. Stamps, and C. M. Hu, Level Attraction Due to Dissipative Magnon-Photon Coupling, Phys. Rev. Lett. **121**, 137203 (2018).

[23] V. L. Grigoryan, K. Shen, and K. Xia, Synchronized spin-photon coupling in a microwave cavity, Phys. Rev. B. **98**, 024406 (2018).

[24] Y. P. Wang, J. W. Rao, Y. Yang, P. C. Xu, Y. S. Gui, B. M. Yao, J. Q. You, and C.-M. Hu, Nonreciprocity and Unidirectional Invisibility in Cavity Magnonics, Phys. Rev. Lett. **123**, 127202 (2019).

[25] J. K. Xie, S. L. Ma, and F. L. Li, Quantum-interference enhanced magnon blockade in an yttrium-iron-garnet sphere coupled to superconducting circuits, Phys. Rev. A **101**, 042331 (2020).

[26] F. Wang, C. Gou, J. Xu, and C. Gong, Hybrid magnon-atom entanglement and magnon blockade via quantum interference, Phys. Rev. A **106**, 013705 (2022).

[27] Z. Jin and Jun Jing, Magnon blockade in magnon-qubit systems, Phys. Rev. A **108**, 053702 (2023).

[28] D. Zhang, X. Q. Luo, Y. P. Wang, T. F. Li, and J. Q. You, Observation of the exceptional point in cavity magnon-polaritons, Nat. Commun. **8**, 1368 (2017).

[29] M. Harder, L. Bai, P. Hyde, and C. M. Hu, Topological properties of a coupled spin-photon system induced by damping, Phys. Rev. B **95**, 214411 (2017).

[30] Y. Cao and P. Yan, Exceptional magnetic sensitivity of PT-symmetric cavity magnon polaritons, Phys. Rev. B **99**, 214415 (2019).

[31] J. Zhao, Y. Liu, L. Wu, C. K. Duan, Y. Liu, and J. Du, Observation of Anti-PT-Symmetry Phase Transition in the Magnon-Cavity-Magnon Coupled System, Phys. Rev. Appl. **13**, 014053 (2020).

[32] G.-Q. Zhang and J. Q. You, Higher-order exceptional point in a cavity magnonics system, Phys. Rev. B **99**, 054404 (2019).
[33] B. Yao, Y. S. Gui, J. W. Rao, S. Kaur, X. S. Chen, W. Lu, Y. Xiao, H. Guo, K. P. Marzlin, and C. M. Hu, Cooperative polariton dynamics in feedback-coupled cavities, Nat. Commun. **8**, 1437 (2017).
[34] M. Tian, M. Wang, G.-Q. Zhang, H.-C. Li, and W. Xiong, Critical cavity-magnon polariton mediated strong long-distance spin-spin coupling, arXiv:2304.13553.
[35] X. L. Hei, X. L. Dong, J. Q. Chen, C. P. Shen, Y. F. Qiao, and P. B. Li, Enhancing spin-photon coupling with a micromagnet, Phys. Rev. A **103**, 043706 (2021).
[36] D. Xu, X.-K. Gu, H.-K. Li, Y.-C. Weng, Y.-P. Wang, J. Li, H. Wang, S.-Y. Zhu, and J. Q. You, Quantum Control of a Single Magnon in a Macroscopic Spin System, Phys. Rev. Lett. **130**, 193603 (2023).
[37] H. Y. Yuan, P. Yan, S. Zheng, Q. Y. He, K. Xia, and M.-H. Yung, Steady Bell State Generation via Magnon-Photon Coupling, Phys. Rev. Lett. **124**, 053602 (2020).
[38] F. X. Sun, S. S. Zheng, Y. Xiao, Q. Gong, Q. He, and K. Xia, Remote Generation of Magnon Schrödinger Cat State via Magnon-Photon Entanglement, Phys. Rev. Lett. **127**, 087203 (2021).
[39] G. Q. Zhang, W. Feng, W. Xiong, Q. P. Su, and C. P. Yang, Generation of long-lived W states via reservoir engineering in dissipatively coupled systems, Phys. Rev. A **107**, 012410 (2023).
[40] S. F. Qi and J. Jing, Generation of Bell and Greenberger-Horne-Zeilinger states from a hybrid qubit-photon-magnon system, Phys. Rev. A **105**, 022624 (2022).
[41] R. Hisatomi, A. Osada, Y. Tabuchi, T. Ishikawa, A. Noguchi, R. Yamazaki, K. Usami, and Y. Nakamura, Bidirectional conversion between microwave and light via ferromagnetic magnons, Phys. Rev. B **93**, 174427 (2016).
[42] N. Zhu, X. Zhang, X. Han, C. L. Zou, C. Zhong, C. H. Wang, L. Jiang, and H. X. Tang, Waveguide cavity optomagnonics for broadband multimode microwave-to-optics conversion, Optica **7**, 1291 (2020).
[43] Y. Tabuchi, S. Ishino, A. Noguchi, T. Ishikawa, R. Yamazaki, K. Usami, and Y. Nakamura, Coherent coupling between a ferromagnetic magnon and a superconducting qubit, Science **349**, 405 (2015).
[44] D. Lachance-Quirion, S. P. Wolski, Y. Tabuchi, S. Kono, K. Usami, and Y. Nakamura, Entanglement-based single-shot detection of a single magnon with a superconducting qubit, Science, **367**, 425 (2020).
[45] O. V. Dobrovolskiy, R. Sachser, T. Brächer, T. Böttcher, V. V. Kruglyak, R. V. Vovk, V. A. Shklovskij, M. Huth, B. Hillebrands, and A. V. Chumak, Magnon–fluxon interaction in a ferromagnet/superconductor heterostructure, Nat. Phys. **15**, 477 (2019).
[46] S. P. Wolski, D. Lachance-Quirion, Y. Tabuchi, S. Kono, A. Noguchi, K. Usami, and Y. Nakamura, Dissipation-Based Quantum Sensing of Magnons with a Superconducting Qubit, Phys. Rev. Lett. **125**, 117701 (2020).
[47] T. Neuman, D. S. Wang, and P. Narang, Nanomagnonic Cavities for Strong Spin-Magnon Coupling and Magnon-Mediated Spin-Spin Interactions, Phys. Rev. Lett. **125**, 247702 (2020).
[48] D. S. Wang, T. Neuman, and P. Narang, Spin Emitters beyond the Point Dipole Approximation in Nanomagnonic Cavities, J. Phys. Chem. C **125**, 6222 (2021).
[49] D. S. Wang, M. Haas, and P. Narang, Quantum Interfaces to the Nanoscale, ACS Nano **15**, 7879 (2021).
[50] I. C. Skogvoll, J. Lidal, J. Danon, and A. Kamra, Tunable anisotropic quantum Rabi model via magnon spin-qubit ensemble, Phys. Rev. Applied **16**, 064008 (2021).
[51] W. Xiong, M. Tian, G.-Q. Zhang, and J. Q. You, Strong long-range spin-spin coupling via a Kerr magnon interface, Physical Review B **105**, 245310 (2022).
[52] L. Trifunovic, F. L. Pedrocchi, and D. Loss, Long-Distance Entanglement of Spin Qubits via Ferromagnet, Phys. Rev. X **3**, 041023 (2013).
[53] M. Fukami, D. R. Candido, D. D. Awschalom, and M. E. Flatté, Opportunities for Long-Range Magnon-Mediated Entanglement of Spin Qubits via On- and Off-Resonant Coupling, PRX Quantum **2**, 040314 (2021).
[54] X. Zhang, C. L. Zou, L. Jiang, and H. X. Tang, Cavity magnomechanics, Sci. Adv. **2**, e1501286 (2016).
[55] J. Li, S.-Y. Zhu, and G. S. Agarwal, Magnon-Photon-Phonon Entanglement in Cavity Magnomechanics, Phys. Rev. Lett. **121**, 203601 (2018).
[56] R.-C. Shen, J. Li, Z.-Y. Fan, Y.-P. Wang, and J. Q. You, Mechanical Bistability in Kerr-modified Cavity Magnomechanics, Phys. Rev. Lett. 129, 123601 (2022).
[57] J. Li, Y.-P. Wang, W.-J. Wu, S.-Y. Zhu, and J. Q. You, Quantum Network with Magnonic and Mechanical Nodes, PRX Quantum **2**, 040344 (2021).
[58] J. Chen, X.-G. Fan, W. Xiong, D. Wang, and L. Ye, Nonreciprocal entanglement in cavity-magnon optomechanics, Phys. Rev. B **108**, 024105 (2023).
[59] J. Chen, X.-G. Fan, W. Xiong, D. Wang, and L. Ye, Nonreciprocal Photon-Phonon Entanglement in Kerr-Modified Spinning Cavity Magnomechanics, Phys. Rev. A **109**, 043512 (2024).
[60] I. Proskurin, A. S. Ovchinnikov, J. Kishine, and R. L. Stamps, Cavity optomechanics of topological spin textures in magnetic insulators, Phys. Rev. B **98**, 220411(R) (2018).
[61] W. Xiong, M. Wang, G.-Q. Zhang, and J. Chen, Optomechanical-interface-induced strong spin-magnon coupling, Phys. Rev. A **107**, 033516 (2023).
[62] Y.-P. Gao, C. Cao, T.-J. Wang, Y. Zhang, and C. Wang, Cavity-mediated coupling of phonons and magnons, Phys. Rev. A **96**, 023826 (2017).
[63] X. Zhang, N. Zhu, C.-L. Zou, and H. X. Tang, Optomagnonic Whispering Gallery Microresonators, Phys. Rev. Lett. **117**, 123605 (2016).
[64] A. Osada, R. Hisatomi, A. Noguchi, Y. Tabuchi, R. Yamazaki, K. Usami, M. Sadgrove, R. Yalla, M. Nomura, and Y. Nakamura, Cavity Optomagnonics with Spin-Orbit Coupled Photons, Phys. Rev. Lett. **116**, 223601 (2016).
[65] J. A. Haigh, A. Nunnenkamp, A. J. Ramsay, and A. J. Ferguson, Triple-Resonant Brillouin Light Scattering in Magneto-Optical Cavities, Phys. Rev. Lett. **117**, 133602 (2016).
[66] G. Q. Zhang, Y. P. Wang, and J. Q. You, Theory of the magnon Kerr effect in cavity magnonics, Sci. China: Phys. Mech. Astron. **62**, 987511 (2019).
[67] Y. P. Wang, G. Q. Zhang, D. Zhang, T. F. Li, C. M. Hu, and J. Q. You, Bistability of Cavity Magnon Polaritons, Phys. Rev. Lett. **120**, 057202 (2018).
[68] S. Zheng, Z. Wang, Y. Wang, F. Sun, Q. He, P. Yan, and H. Y. Yuan, Tutorial: Nonlinear magnonics, J. Appl. Phys. **134**, 151101 (2023).
[69] R. C. Shen, Y. P. Wang, J. Li, S. Y. Zhu, G. S. Agar-

wal, and J. Q. You, Long-Time Memory and Ternary Logic Gate Using a Multistable Cavity Magnonic System, Phys. Rev. Lett. **127**, 183202 (2021).

[70] F.-Z. Ji and J.-H. An, Kerr-Nonlinearity-Induced Strong Spin-Magnon Coupling, Phys. Rev. B **108**, L180409 (2023).

[71] G. Liu, W. Xiong, and Z. J. Ying, Switchable superradiant phase transition with Kerr magnons, Phys. Rev. A **108**, 033704 (2023).

[72] G.-Q. Zhang, Y. Wang, and W. Xiong, Detection sensitivity enhancement of magnon Kerr nonlinearity in cavity magnonics induced by coherent perfect absorption, Phys. Rev. B **107**, 064417 (2023).

[73] J. M. P. Nair, D. Mukhopadhyay, and G. S. Agarwal, Enhanced sensing of weak anharmonicities through coherences in dissipatively coupled anti-PT symmetric systems, Phys. Rev. Lett. **126**, 180401 (2021).

[74] C. Kong, H. Xiong, and Y. Wu, Magnon-Induced Nonreciprocity Based on the Magnon Kerr Effect, Phys. Rev. Applied **12**, 034001 (2019).

[75] W. Xiong and Z. Li, Highly-tunable and strong nonreciprocity in coupled nonlinear cavity magnonics, arXiv:2309.09245.

[76] M. Wang, C. Kong, Z.-Y. Sun, D. Zhang, Y.-Y. Wu, and L.-L. Zheng, Nonreciprocal high-order sidebands induced by magnon Kerr nonlinearity, Phys. Rev. A **104**, 033708 (2021).

[77] R. Huang, A. Miranowicz, J. Q. Liao, F. Nori, and H. Jing, Nonreciprocal Photon Blockade, Phys. Rev. Lett. **121**, 153601 (2018).

[78] Y. F. Jiao, S. D. Zhang, Y. L. Zhang, A. Miranowicz, L. M. Kuang, and H. Jing, Nonreciprocal optomechanical entanglement against backscattering losses, Physical Review Letters **125**, 143605 (2020).

[79] Wei Zhang, Tie Wang, Shutian Liu, Shou Zhang, and Hong-Fu Wang, Nonreciprocal photon blockade in a spinning resonator coupled to two two-level atoms. Sci. China Phys. Mech. Astron. **66**, 240313 (2023).

[80] Y. W. Jing, H. Q. Shi, and X. W. Xu, Nonreciprocal photon blockade and directional amplification in a spinning resonator coupled to a two-level atom, Phys. Rev. A **104**, 033707 (2021).

[81] X. Y. Yao, H. Ali, and P. B. Li, Nonreciprocal Phonon Blockade in a Spinning Acoustic Ring Cavity Coupled to a Two-Level System, Phys. Rev. Applied **17**, 054004 (2022).

[82] Y. Wang, W. Xiong, Z. Xu, G. Q. Zhang, and J. Q. You, Dissipation-induced nonreciprocal magnon blockade in a magnon-based hybrid system, Sci. China Phys. Mech. Astron. **65**, 260314 (2022).

[83] A. J. Shields, Semiconductor quantum light sources, Nat. Photon. **1**, 215 (2007).

[84] L. Davidovich, Sub-Poissonian processes in quantum optics, Rev. Mod. Phys. **68**, 127 (1996).

[85] A. Imamoğlu, H. Schmidt, G. Woods, and M. Deutsch, Strongly Interacting Photons in a Nonlinear Cavity, Phys. Rev. Lett. **79**, 1467 (1997).

[86] K. M. Birnbaum, A. Boca, R. Miller, A. D. Boozer, T. E. Northup, and H. J. Kimble, Photon blockade in an optical cavity with one trapped atom, Nature **436**, 87 (2005).

[87] Y. H. Zhou, H. Z. Shen, X. Y. Zhang, and X. X. Yi, Zero eigenvalues of a photon blockade induced by a non-Hermitian Hamiltonian with a gain cavity, Phys. Rev. A **97**, 043819 (2018).

[88] C. Hamsen, K. N. Tolazzi, T. Wilk, and G. Rempe, Two-photon blockade in an atom-driven cavity QED system, Phys. Rev. Lett. **118**, 133604 (2017).

[89] H. Z. Shen, Y. H. Zhou, and X. X. Yi, Tunable photon blockade in coupled semiconductor cavities, Phys. Rev. A **91**, 063808 (2015).

[90] Y. H. Zhou, H. Z. Shen, X. Q. Shao, X. X. Yi, Strong photon antibunching with weak second-order nonlinearity under dissipation and coherent driving, Opt. Express **24**, 17332 (2016).

[91] M. Bamba, A. Imamoğlu, I. Carusotto, and C. Ciuti, Origin of strong photon antibunching in weakly nonlinear photonic molecules, Phys. Rev. A **83**, 021802 (2011).

[92] Y. H. Zhou, H. Z. Shen, and X. X. Yi, Unconventional photon blockade with second-order nonlinearity, Phys. Rev. A **92**, 023838 (2015).

[93] H. Flayac, and V. Savona, Unconventional photon blockade, Phys. Rev. A **96**, 053810 (2017).

[94] H. J. Snijders, J. A. Frey, J. Norman, H. Flayac, V. Savona, A. C. Gossard, J. E. Bowers, M. P. van Exter, D. Bouwmeester, and W. Löffler, Observation of the unconventional photon blockade, Phys. Rev. Lett. **121**, 043601 (2018).

[95] J. T. Hou and L. Liu, Strong coupling between microwave photons and nanomagnet magnons, Phys. Rev. Lett. **123**, 107702 (2019).

[96] N. Kostylev, M. Goryachev, and M. E. Tobar, Superstrong coupling of a microwave cavity to yttrium iron garnet magnons, Appl. Phys. Lett. **108**, 062402, (2016).